Received January 26, 2019, accepted February 22, 2019, date of publication March 7, 2019, date of current version March 20, 2019.

Digital Object Identifier 10.1109/ACCESS.2019.2901957

A Novel CAP-WDM-PON Employing Multi-Band DFT-Spread DMT Signals Based on Optical Hilbert-Transformed SSB Modulation

YOUXU ZENG, ZE DONG, YIFAN CHEN, XINXING WU, HAILIAN HE, JIALIN YOU, AND QINGHUA XIAO

College of Information Science and Technology, Huaqiao University, Xiamen 361021, China

Corresponding author: Ze Dong (zdong9@hqu.edu.cn)

This work was supported in part by the Natural Science Foundation of China under Grant 61401166, in part by the Fujian Province Science Fund for Distinguished Young Scholars under Grant 2016J06015 (11166004), in part by the Quanzhou Science and Technology Project under Grant 2018C116R, and in part by the Fundamental Research Funds for the Central Universities ZQN-YX305.

ABSTRACT We propose and experimentally demonstrate a novel carrier-less amplitude/phase modulation wavelength-division-multiplexing passive optical network (CAP-WDM-PON) with its bandwidth efficiency enhanced by using a multi-band discrete Fourier transform spread (DFT-spread) discrete multi-tone (DMT) signal based on Hilbert-transformed single-sideband (HB-SSB) modulation. The DFT-spread technique is utilized to extend orthogonal subcarriers, which effectively restrain the high-peak signal formation probability, and thereby, it can significantly reduce the high peak-to-average power ratio of the DMT signal. The proposed optical line terminal (OLT) in CAP-WDM-PON suggests five downlink optical subcarriers. For each optical subcarrier, there are as many as 6 × 20 Gb/s SSB digital DMT channels CAP modulated on them, which can be efficiently generated by using only one set of optical transmitter hardware. The experimental results show that the proposed system is capable of accommodating 5 × 6 channels (20 Gb/s per channel) within an optical distribution network (ODN) loss budget of 19.4 dB, and there is a 2.4-dB ODN loss budget improvement by utilizing the DFT-spread scheme. More importantly, the proposed spectral- and bandwidth-efficient CAP-WDM-PON system requires six times less downlink optical transmitters at the OLT, which can be translated into savings in cost, power consumption, and footprint. In addition, key techniques, such as pre-equalization for high-frequency components and digital HB-SSB modulation format for generation of multi-band DMT signals, are also studied.

INDEX TERMS WDM-PON, CAP, DFT-Spread, Hilbert transform, single sideband modulation, pre-equalization.

I. INTRODUCTION

Wavelength division multiplexing passive optical network (WDM-PON) with dedicated more than 10 Gb/s per channel or user is expected to meet the huge capacity and high spectral efficiency (SE) demands in next-generation heterogeneous access networks [1]–[5]. Optical Nyquist-WDM, carrier-less amplitude/phase modulation (CAP), and orthogonal frequency division modulation (OFDM) are the most popular and promising multiplexing techniques to realize high SE WDM-PON [6]. Although OFDM and Nyquist-WDM systems based on optical coherent detection present excellent receiver sensitivity, the high cost of coherent detection coupled to ONUs remains the problem to be addressed [7]. In recent years, discrete multi-tone (DMT) with relative lower system complexity and higher SE based on cost-effective intensity modulation/direct detection (IM/DD) has attracted a lot of attention in WDM-PON. DMT is a multi-carrier scheme which derives from OFDM, with its signals regarded as a special type of OFDM signals with the corresponding imaginary parts equaling zero. It inherits all the advantages of OFDM signals, such as the transparency to modulation formats, and robustness tolerance to chromatic dispersion and polarization mode dispersion, is considered as a promising candidate for the future WDM-PON system [8]–[18]. However, as a drawback of multiple orthogonal subcarriers architecture,

The associate editor coordinating the review of this manuscript and approving it for publication was Miaowen Wen.

the high peak-to-average power ratio (PAPR) issue makes the DMT signal very susceptible to the optical fiber nonlinear effects [19]. For the aim to serve more optical network units (ONUs), effective PAPR deduction is expected for this kind of access networks adopting DMT signals to obtain superior receiver power sensitivity (RPS) and sufficient system loss budget.

There are several PAPR deduction methods based on amplitude clipping law such as selective mapping (SLM), partial transmission sequence, constant envelope, u-law expansion, coding-class method and so on [20]–[22]. Different from the amplitude clipping method, the DFT-spread, extends spectrum mapping of each data symbol onto all allocated DMT subcarriers for its PAPR deduction with one additional FFT/IFFT processing, has attracted a lot of attention in recent years [18]. On the one hand, it is advantageous for DFT-spread DMT that the similar power spectrum with single carrier frequency division multiple access (SC-FDMA) and relatively lower computational complexity can help to decrease the PAPR without signal-to-noise (SNR) loss [23]–[26].

On the other hand, as an effective modulation technique developed from classical double-sideband (DSB), single-sideband (SSB) modulation effectively utilizes only the half bandwidth of DSB, and it thus can further improve the system bandwidth- and spectral efficiency [27], [28]. However, most of the optical SSB techniques applied today are based on the preserving of rich low-frequency components that require expensive optical filtering.

In this paper, we propose and experimentally demonstrate a CAP-WDM-PON with its bandwidth- and spectral efficiency enhanced by employing multi-band DFT-spread DMT signals based on optical Hilbert-transformed SSB (HB-SSB) modulation format. To simplify the architecture with multi-level multi-band quadrature amplitude modulation (QAM) by matched Nyquist filter pairs in the previous work [4], in our scheme, the square spectral characteristics of DMT signals and Hilbert transform are utilized to guarantee higher signal integrity and system SE. It is advantageous in the proposed CAP-WDM-PON that the significantly reduced PAPR for each DMT signal can help to improve system tolerance to fiber nonlinear effect. Resultantly, the optimized launch fiber power can be shared for loss budget requirement with a certain OLT ports. The CAP-WDM-PON with direct detection supporting 30 ONU channels with 6 × 20-Gb/s digital downlink channels sharing one wavelength, i.e., 6 × 20-Gb/s downlink channels per optical transmitter is implemented at the OLT. Such highly-efficient bandwidth utilization is enabled by multi-band CAP processing, HB-SSB, and reference-based pre-equalization. All these operations are performed through only one high-speed digital-to-analog converter (DAC) in digital domain. The 30 ONU channels can be divided as follows: 5 continuous wavelength (CW) emitted by 5 lasers at the OLT, and 6 digital CAP multi-band SSB channels per CW, with amounting to 20-Gb/s DMT signal employing DFT-spread 16QAM for each channel. When the bit error ratio (BER) is less than the pre-FEC limit of 2×10^{-2} [29], an optical distribution networks (ODN) loss budget of 19.4 dB is achieved for the proposed IM/DD based CAP-WDM-PON and 2.4-dB launch fiber power is optimized by employing DFT-spread technique. The remainder of this paper is organized as follows. Section II shows the principle for the CAP-WDM-PON, multi-band DFT-spread DMT generation, optical HB-SSB, and reference-based pre-equalization scheme; Section III orderly describes the proof-of-concept experimental setup and results; Finally, section IV draws the conclusion of this work.

II. PRINCIPLE

A. THE PRINCIPLE FOR CAP-WDM-PON EMPLOYING MULTI-BAND DFT-SPREAD DMT AND HB-SSB

The principle of the spectrum- and bandwidth-efficient CAP-WDM-PON employing multi-band DFT-Spread 16QAM DMT signal based on HB-SSB is shown in Fig. 1. At the OLT, the continuous wave (CW) emitted from the lasers are modulated via the intensity modulator (IM) driven by CAP multi-band DMT signal based on HB-SSB. The principle for DFT-spread DMT channel generation is shown in Fig. 1(a). Firstly, the pseudo random binary sequence (PRBS) data stream is subjected to 16QAM mapping after serial-to-parallel conversion in digital domain; Secondly, the digital 16QAM signal $\{X_{\mathrm{m}}, m = 0, 1, \ldots, M-1\}$ is frequency-extended by M-point DFT. Finally, the (N-M)-point sub-carrier mapping, IFFT transform for N-subcarrier mapped signal, and 1/8 tail of sequence addition for cyclic prefix (CP) processing are implemented to obtain the electrical DFT-spread 16QAM DMT signal. Fig. 1(b) shows the principle for the generation of CAP multi-band DMT signal based on HB-SSB. The generated DMT channels are up-converted independently to obtain desired positive (P) or negative (N) frequency bands. The rectangular profile of the spectrum for DMT signal can avoid the crosstalk from the adjacent channels. Compared with the DSB case shown in Fig. 1(c), the CAP multi-band DMT signal based on HB-SSB carries 6 SSB digital channels, each of which carries 5-Gbaud 16QAM DMT signal, with double bandwidth utilization and spectral efficiency. The guard band between adjacent DMT channels is set as 0.1 GHz, and the overall occupied RF bandwidth of 6 SSB DMT channels is 14.8 GHz. The downlink signals are transmitted through a classic splitter-based ODN, and are then directly-detected by a photo detector (PD) at the ONU. The PD outputs are digitalized by ADCs with at least 2.5-GHz bandwidth and 10-Gsa/s sample rate. For the digital signal processing (DSP), one of the multi-band SSB DMT channels is processed for down-conversion to obtain an independent channel of the DMT signal. For de-modulation of the base-band DMT signal, cyclic prefix removal, serial-to-parallel conversion (S/P), FFT processing, inverse mapping for sub-carriers, IFFT processing, 16QAM de-mapping, parallel-to-serial conversion (P/S), decoding and final BER calculation are implemented in the DSP block. It is worth noting that our

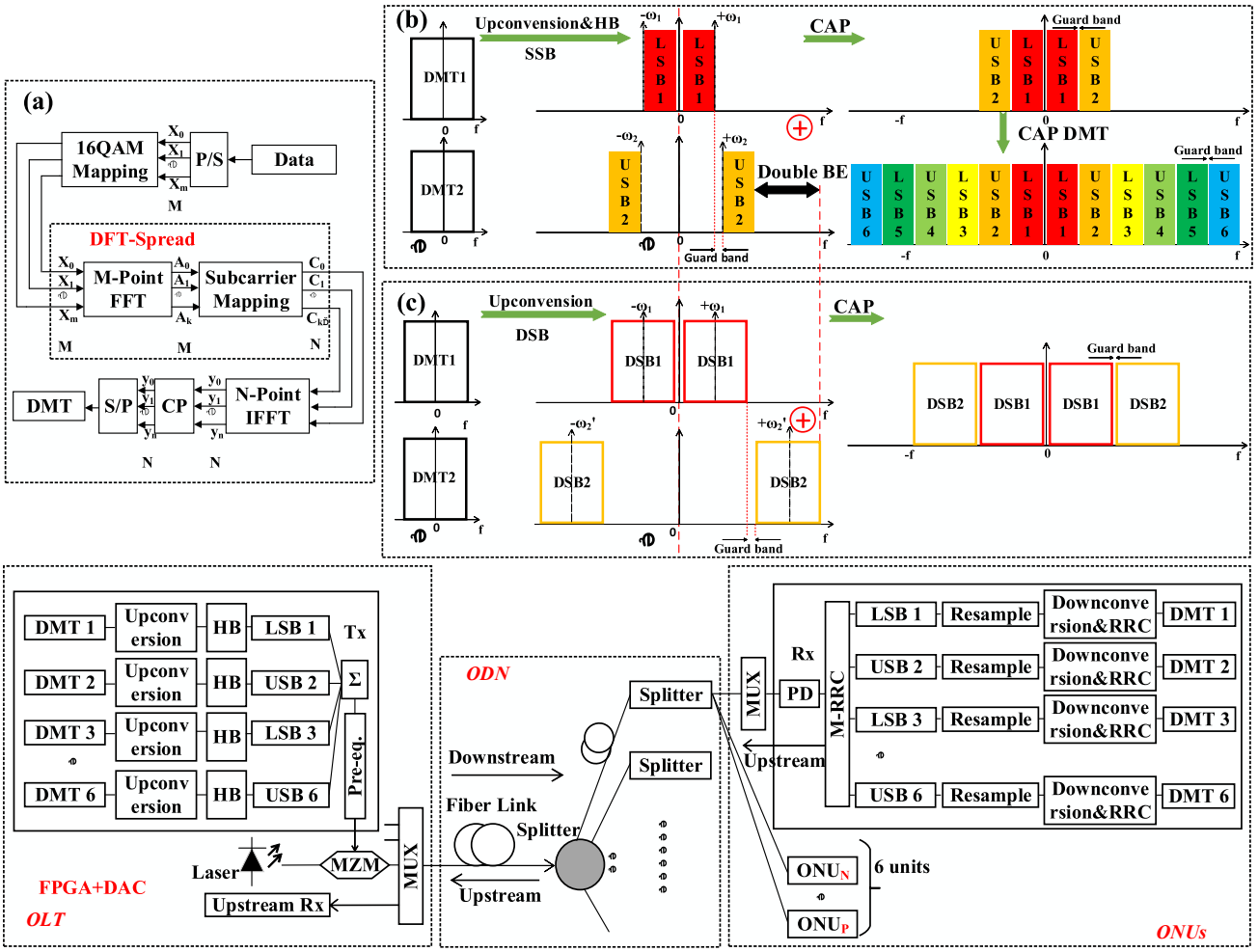

FIGURE 1. Principle for the CAP-WDM-PON employing DFT-spread DMT based on HB-SSB, MZM: Mach-Zehnder modulator, (a): principle of DMT signal generation based on DFT-spread, (b): schematic diagram of Multi-band CAP signal generation based on HB-SSB, (c): schematic diagram of Multi-band CAP signal generation based on DSB.

scheme with DMT-WDM-PON for downstream is compatible with the upstream in other typical PON structures.

B. THE GENERATION OF DFT-SPREAD DMT SIGNAL BASED ON CENTRALIZED MAPPING

There are two common subcarrier mapping schemes for DFT-spread, classified as scattered and centralized mapping as shown in Fig. 2(a) and (b). The scattered mapping scheme is to load the data onto the discontinuous subcarriers by DFT transform, while the centralized one is to load the DFT output data onto continuous subcarriers with the rest of the subcarriers set as zero by zero padding. However, the inter-subcarrier interference with scattered mapping is formed once slight frequency offsets for the subcarriers occur.

A DMT signal consists of multiple independently orthogonal subcarriers. High PAPR issue occurs when subcarriers are added up coherently, which will increase the processing burden of digital-to-analog converter and modulator due to resultant DMT signal distortion and high bit error ratio. The

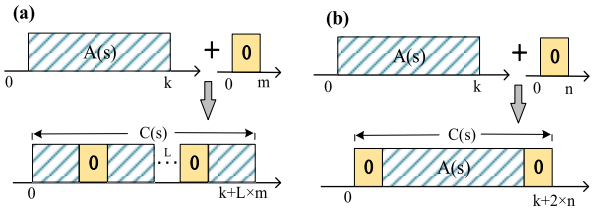

FIGURE 2. (a) Scattered mapping. (b) Centralized mapping.

PAPR can be defined as

$$\text{PAPR} = \frac{\max |x(k)|^2}{E\{|x(k)|^2\}} \tag{1}$$

As shown in Fig. 1(a), the DMT architecture is assumed to be formed by centralized mapping, which means that there are subcarriers in a total of N. The number of subcarriers with data is M, and the number of those without data for intervals between adjacent subcarriers is Q. So $N = M + Q$. $\{A_k, k = 0, 1, \ldots, M-1\}$ represents the frequency sampled data after

FFT of the original input data $\{X_m, m = 0, 1, \ldots, M-1\}$. $\{C_{k'}, k' = 0, 1, \ldots, N-1\}$ is the sampled data after sub-carrier mapping in frequency domain, and then DMT signal $y_n = 0, 1, \ldots, N-1$ is obtained by IFFT processing. The frequency-domain sampled signal after subcarrier dispersion mapping can be expressed as:

$$c_k = \begin{cases} A_{l/Q} & l = Q \times k (0 \le k \le M-1) \\ 0 & otherwise \end{cases} \tag{2}$$

$\{y_n\}$ is the data of $\{c_k\}$ after IFFT in time domain.

$$y_n = \frac{1}{Q}\left\{\frac{1}{M}\sum_{k=0}^{M-1} A_k e^{j2\pi \frac{m}{M}k}\right\}, \quad n = 1, 2, \ldots, kQ-1 \tag{3}$$

According to eq. 2 and 3, the data $\{y_n\}$ in time domain obtained by IFFT is a sampling shift of original input data $\{X_m\}$. Therefore, the PAPR of the DMT signal after sub-carrier scattered mapping is approaching to that of the traditional single-carrier signal.

In order to estimate the statistical characteristics of PAPR in DMT signal, the concept of complementary cumulative distribution function (CCDF) represent the probability that PAPR exceeds a certain value of $PAPR_0$.

$$CCDF = 1 - (1 - e^{-PAPR_0})^N \tag{4}$$

where N is the number of subcarriers.

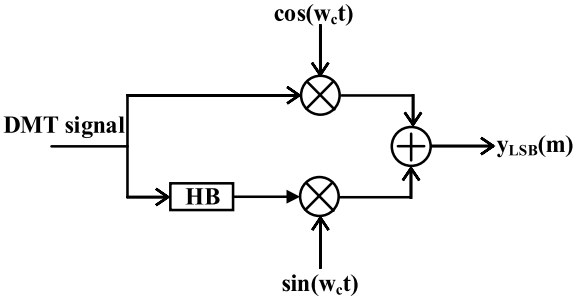

FIGURE 3. Principle for single band case of the multi-band DMT signal generation adopting HB-SSB.

C. THE GENERATION OF CAP MULTI-BAND DMT SIGNAL BASED ON HB-SSB

Fig. 1(b) show the principle and corresponding spectral transformation for the generation of CAP multi-band DMT signal based on HB-SSB. In order to theoretically demonstrate the principle for single band case of the multi-band DMT signal generation adopting HB-SSB shown in Fig. 3, we assume that the DMT signal is $m(t) = A_m \cos \omega_m t$, and the carrier is $c(t) = \cos \omega_c t$, in which ω_m and ω_c respectively indicate the single angular frequency of the DMT signal and the carrier. The CAP multi-band DMT signal based on DSB can be expressed as:

$$\begin{aligned} S_{DSB}(t) &= A_m \cos \omega_m t \cos \omega_c t \\ &= \frac{1}{2} A_m \cos(\omega_m + \omega_c)t + \frac{1}{2} A_m \cos(\omega_c - \omega_m)t \end{aligned} \tag{5}$$

By HB processing implementation for $m(t) = A_m \cos w_m t$ and $\hat{m}(t) = A_m \sin w_m t$ in eq. 5, the reserved upper or lower sideband can be expressed as the HB-SSB DMT as follows:

$$S_{SSB}(t) = \frac{1}{2} m(t) \cos \omega_c t \pm \frac{1}{2} \hat{m}(t) \sin(\omega_c t) \tag{6}$$

where $\hat{m}(t)$ is the HB transform for $m(t)$.

D. PRE-EQUALIZATION BASED ON REFERENCE SIGNAL

For the key components at the optical transmitter of OLT, such as DAC, MZM, and EA, digital reference-based pre-equalization is utilized to compensate for the high frequency components loss. An on-off keying (OOK) signal is used as the reference signal to be transmitted in the back-to-back (BTB) link. Assuming that S_{ref} and R_{ref} respectively denote the transmitted and received OOK signals in frequency domain, the linear channel transfer function (TF) can be defined as:

$$H_{TF} = S_{ref.}/R_{ref} \tag{7}$$

If the transmitted signal S (DFT-spread 16QAM DMT signal) is processed as:

$$S_{pre-eq.} = S \cdot H_{TF} \tag{8}$$

the impairment of high frequency component caused by bandwidth limitation can be accurately pre-compensated. In order to avoid expensive long-sized FFT processing in practical application, the pre-equalization scheme is implemented by using the convolution of the time-domain TF and the transmitted CAP multi-band DMT signal

$$s_{pre-eq.} = s * h_{TF} \tag{9}$$

In our scheme, the continuous-wavelength (CW) light-waves emitted from external cavity lasers (ECL) are with the linewidth of less than 100 kHz. To simplify the re-sampling process, a 25-Gbaud (as an integer multiple of the DAC sampling rate of 50 Gsa/s) OOK reference signal is applied to pass through the optical transmitter at the OLT in back to back (BTB) link. A digital storage oscilloscope (OSC) with the sampling rate of 50 GSa/s and the bandwidth of 17 GHz is utilized to realize the analog-to-digital conversion (ADC) and the data capture after optical-to-electrical (O/E) conversion. Clock recovery is used to compensate for the impairment by the rate of 2 samples/symbol of the DAC. The average of 5 sets of OOK signals with the PRBS length of $2^{15}-1$ is used to increase the accuracy before the time-domain synchronization between the recovered pattern and the known OOK pattern. The transmitted binary data after FFT are divided by the received ones after FFT in frequency domain to obtain the TF. Then, the CAP multi-band DMT signals based on HB-SSB is used to convolve with the TF in time domain for pre-equalization.

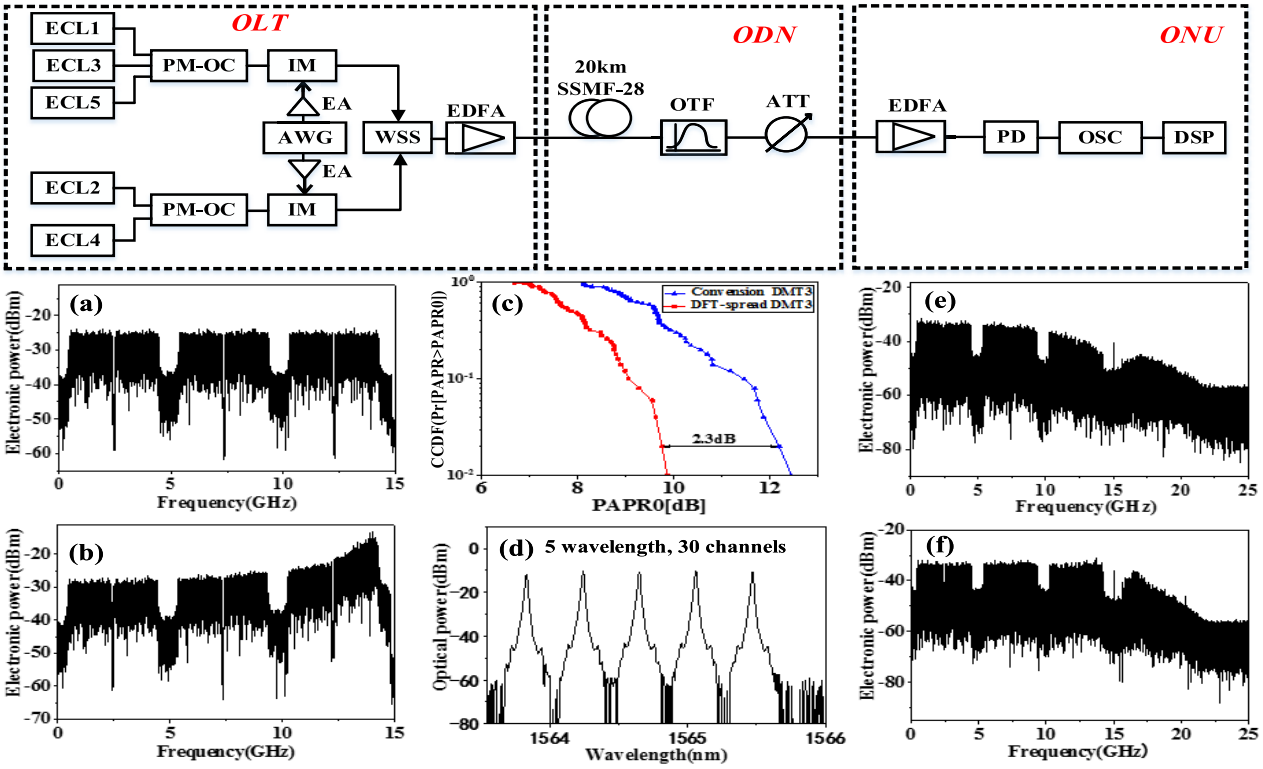

FIGURE 4. The proof-of-concept experimental setup for the downstream of direct CAP-WDM-PON employing multi-band DFT-Spread DMT signal and HB-SSB. PM-OC: polarization-maintenance optical coupler, WSS: wavelength selector switch, EDFA: erbium-doped fiber amplifier, OTF: optical tunable filter, ATT: optical attenuator. (a) and (b) Electrical spectra of the multi-band DMT signals before and after pre-equalization, (c) CCDF distribution by DFT-spread, (d) optical spectrum of CAP-WDM-PON offering 30 CAP multi-band DMT channels over 20-km SSMF transmission, (e) and (f) electrical spectra of the multi-band DMT signals before and after pre-equalization at ONU.

III. EXPERIMENTAL SETUP AND RESULTS

The proof-of-concept experimental setup for the downstream of CAP-WDM-PON offering 30 ONUs based on multi-band DFT-spread DMT signal and HB-SSB is shown in Fig. 4. The electrical CAP DFT-spread 16QAM DMT based on HB-SSB is generated by an AWG (Tek70001A) with a sampling rate of 30-GSa/s and a 3-dB bandwidth of 18 GHz. After the power amplification by two electrical amplifiers (EAs) with the 3-dB bandwidth of 40 GHz, the data and $\overline{data}$ outputs of the AWG are used to modulate the odd and the even CWs generated by 5 ECLs with a frequency spacing of 50 GHz via two intensity modulators (IMs). The IM with the 3-dB bandwidth of 40 GHz and the half-wave voltage of 3 V is biased at the linear point of 1.03V. The ECLs are with the output power of 13.5 dBm and the linewidth of less than 100 kHz. The odd and the even CWs are combined by two polarization-maintenance optical couplers (PM-OC) before modulation. The generation of subcarriers for total 30 channels is realized as described in the section above. The pre-equalization is utilized to fully compensate for the bandwidth limitation and linear distortion caused by AWG, EAs and IM at the optical transmitter. The electrical spectra of the 6×20-Gb/s 16QAM signal before and after pre-equalization are respectively shown in Fig. 4(a) and (b). The CCDF curves of DFT-spread based and conventional optical DMT transmission system are depicted in Fig. 4(c). It evidently shows at least 2.3-dB PAPR deduction for optical DMT system by DFT-spread scheme at the CCDF of 2×10^{-2}. Obviously, the high-frequency components within the range of 7.5∼15 GHz are clearly emphasized by pre-equalization. Then one programmable wavelength selective switch (WSS) is used to combine the odd and the even channels, and to flatten the amplitude of each subcarrier. The amplitude and the wavelength bandwidth of each channel in the WSS are fully tunable. The optical spectrum of the CAP-WDM-PON downstream signal is shown as Fig. 4(d). After the optical power amplification by EDFA, the CAP-WDM-PON downstream signal is launched into 20-km standard single-mode fiber (SSMF) with the loss of 4 dB and the chromatic dispersion (CD) of 17ps/km/nm at 1550 nm. The total signal launch fiber power is 10.4 dBm (3.4 dBm per optical subcarrier). At the ONU, O/E conversion for the signal is realized by a PD with a 3-dB bandwidth of 40 GHz. The A/D conversion and the data capture are realized in the storage oscilloscope (OSC, Tek DPO72004C) with a sampling rate of 50 Gs/s and a 3-dB electrical bandwidth of 16 GHz. Fig. 4(e) and (f) respectively illustrate the electrical spectra of the received CAP-WDN-PON signal at 1564.65 nm without and with pre-equalization. It can be seen that the electrical spectrum for CAP multi-band signal with pre-equalization

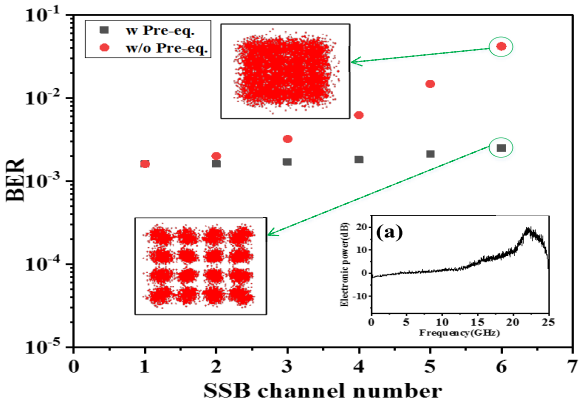

FIGURE 5. BER performance in BTB link for all multi-band DMT channels at 1564.65 nm (received power = −16 dBm) with and without pre-equalization. (a) Reversed channel TF.

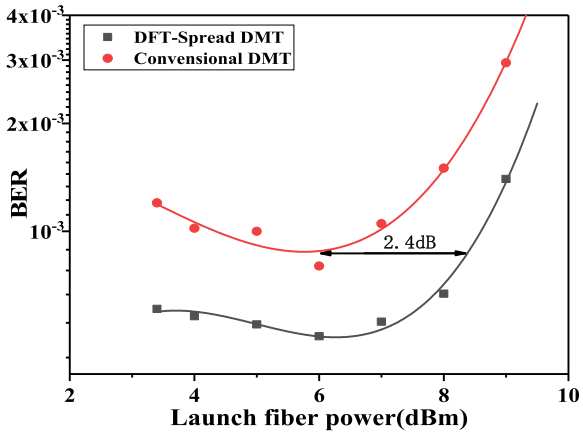

FIGURE 7. BER performance for optical DMT signal versus launch fiber power (received power = −12 dBm) over 20-km SSMF transmission.

after 20-km SSMF transmission is still with flat profile, which guarantees that the DMT channels in high frequency would not be attenuated.

The BER performance of WDM subcarriers (6 channels, average BER) is measured at 1564.65 nm with amounting to 6 × 39600 bits. Fig. 5 shows the BER performance in BTB link for all 6 sub-channels at the received power of −16 dBm with and without pre-equalization. The measured reversed channel TF is inset as Fig. 5(a). It is intuitive that the poor performance for the high frequency components of sub-channels due to the bandwidth limitation of DAC, is fully compensated by pre-equalization. The corresponding constellation diagrams of 16QAM DMT signal with and without pre-equalization are inserted in Fig. 5. According to the BER performance and the corresponding constellation diagram of channel 6, it is evident that the performance of the pre-equalized 16QAM DMT signal is much better than the one without pre-equalization. Fig. 6 shows the BER performance for the 4th DMT channel of subcarrier at 1564.65 nm. At the BER of 2×10^{-2}, the required received power before 20-km SSMF transmission and that after the transmission are −20.05 and −18.95 dBm, which indicates 1.1-dB power penalty by fiber nonlinear effect. By adopting various launch fiber power, the average BER performance comparison for the CAP DMT channels at 1564.65 nm with and without DFT-spread technique is shown in Fig. 7. At the launch fiber power of 5.9 dBm, the BER performance for conventional DMT and that for DFT-Spread DMT are 8×10^{-2} and 5×10^{-2}, respectively. As the launch fiber power continues to increase, the high PAPR leads to obvious BER performance decrease for the conventional DMT without DFT-spread technique. The optical DFT-spread DMT, benefiting from the PAPR reduction, exhibits enhanced BER receiver power sensitivity (RPS) until the launch fiber power increases to 8.3 dBm. Compared with the system employing conventional DMT, there is 2.4-dB fiber nonlinear effect tolerance improvement by utilizing DFT-spread at the BER of 1×10^{-3}. Fig. 8 shows the BER performance for the CAP-WDM-PON employing multi-band DFT-spread DMT based HB-SSB over

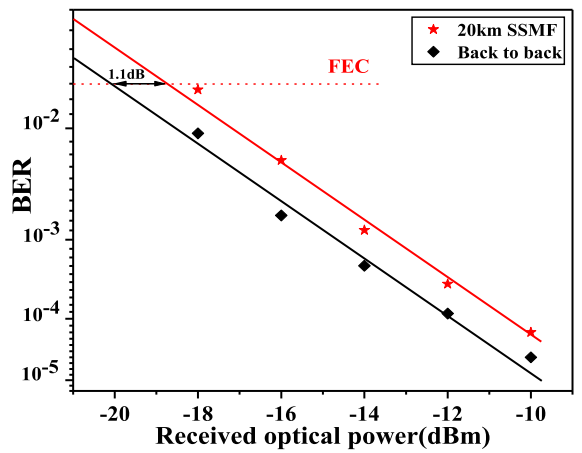

FIGURE 6. Average BER of the downstream signal before and after 20-km SSMF transmission versus received optical power (launch fiber power = 3.4 dBm).

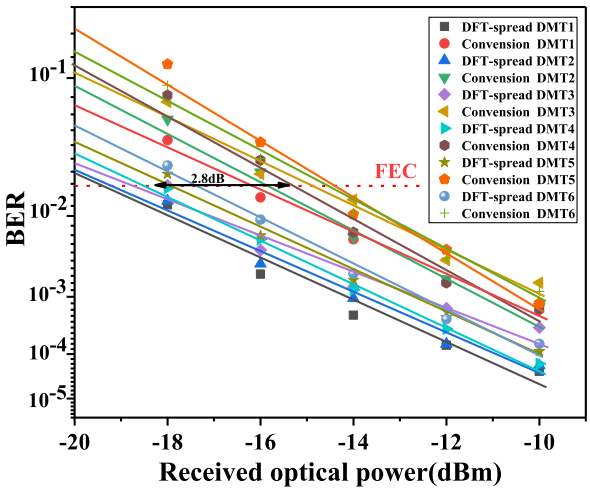

FIGURE 8. BER performance for Optical DMT versus received optical power (launch fiber power = 3.4 dBm) over 20-km SSMF transmission.

20-km SSMF transmission. Obviously, the results indicate that at the BER of 2×10^{-2}, the received optical power for the conventional 16QAM DMT signal and DFT-spread 16QAM DMT are -15.4 and -18.2 dBm, respectively. 2.8-dB RPS is improved by the DFT-spread because of the PAPR deduction for DMT signal. Fig. 9 shows the measured the BER performance for the 5 WDM subcarriers over 20-km SSMF transmission with the received power of -16 dBm per channel. After 20-km SSMF transmission, the BER for all channels is less than the enhanced soft-decision pre-FEC limit of 2×10^{-2} [29]. The constellation for the $+9^{th}$ sub-user at 1564.3 nm and the optical spectrum (Resolution: 0.1 nm) of the CAP-WDM-PON signal after the transmission over 20-km SSMF are also inserted as Fig. 9(a) and (b).

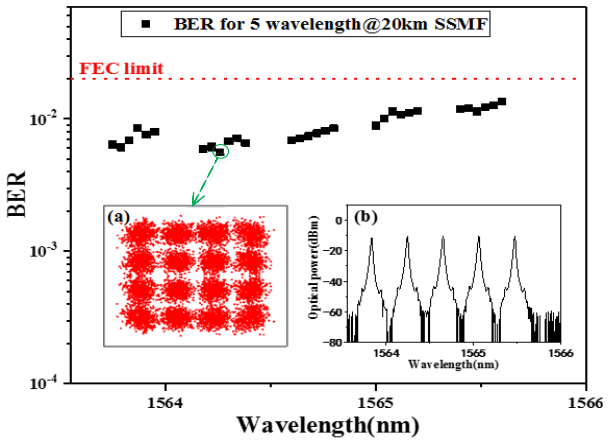

FIGURE 9. BER performance for all 5 wavelengths(received power = −16 dBm) over 20-km SSMF transmission.

IV. CONCLUSION

We have proposed and experimentally demonstrated a bandwidth-efficient directly-detected CAP-WDM-PON system by employing Hilbert transform based multi-band SSB DFT-spread DMT signals. A pre-equalization scheme based revised channel transfer function is employed to accurately pre-compensate for the high frequency loss for the electro-optical components of the signal caused by DAC, optical modulators and electrical drivers at the OLT. For the throughput of 30 downstream channels with 20-Gb/s CAP-WDM-PON, all channels can be served simultaneously. Compared with the conventional DMT technique alone, 2.8-dB system optical receiver sensitivity enhancement and 2.4-dB optical fiber nonlinear effect tolerance improvement by the DFT-spread technique can be obtained, which can provide abundant system loss budget for the legacy ODNs.

REFERENCES

[1] J. D. Reis *et al.*, "Terabit+ (192×10 Gb/s) nyquist shaped UDWDM coherent PON with upstream and downstream over a 12.8 nm band," *J. Lightw. Technol.*, vol. 32, no. 4, pp. 729–735, Feb. 15, 2014.

[2] N. Cvijetic, M.-F. Huang, E. Ip, Y.-K. Huang, D. Qian, and T. Wang, "1.2 Tb/s symmetric WDM-OFDMA-PON over 90km straight SSMF and 1:32 Passive split with digitally-selective ONUs and coherent receiver OLT," in *Proc. OFC/NFOEC*, 2011, pp. 1–3, Paper PDPD7.

[3] H. Rohde, E. Gottwald, P. Alves, C. Oliveira, I. Dedic, and T. Drenski, "Digital multi-wavelength generation and real time video transmission in a coherent ultra dense WDM PON," in *Proc. OFC/NFOEC*, 2013, pp. 1–3, Paper OM3H.3.

[4] J. Zhang, J. Yu, F. Li, N. Chi, Z. Dong, and X. Li, "11×5×9.3 Gb/s WDM-CAP-PON based on optical single-side band multi-level multi-band carrier-less amplitude and phase modulation with direct detection," *Opt. Express*, vol. 21, no. 16, pp. 18842–18848, 2013.

[5] M. Noda *et al.*, "Super-splits 10G-EPON system: 256 ONU passive splits with 240 ns dual-rate burst-mode 3R synctime and bi-directionally extended 35.9 dB loss budgets," in *Proc. OFC/NFOEC*, 2012, pp. 1–3, Paper PDP5B.9.

[6] G. Bosco, A. Carena, V. Curri, P. Poggiolini, and F. Forghieri, "Performance limits of Nyquist-WDM and CO-OFDM in high-speed PM-QPSK systems," *IEEE Photon. Technol. Lett.*, vol. 22, no. 15, pp. 1129–1131, Aug. 1, 2010.

[7] Z. Dong, H. C. Chien, J. Yu, J. Zhang, L. Cheng, and G. K. Chang, "Very-high-throughput coherent ultradense WDM-PON based on Nyquist-ISB modulation," *IEEE Photon. Technol. Lett.*, vol. 27, no. 7, pp. 763–766, Apr. 1, 2015.

[8] R. Ullah *et al.*, "Flattened optical multicarrier generation technique for optical line terminal side in next generation WDM-PON supporting high data rate transmission," *IEEE Access*, vol. 6, pp. 6183–6193, 2018.

[9] Z. Cao, J. Yu, W. Wang, L. Chen, and Z. Dong, "Direct-detection optical OFDM transmission system without frequency guard band," *IEEE Photon. Technol. Lett.*, vol. 22, no. 11, pp. 736–738, Jun. 1, 2010.

[10] R. Deng, J. He, M. Chen, Y. Liu, and L. Chen, "Real-time LR-DDO-OFDM transmission system using EML with 1024-point FFT," *IEEE Photon. Technol. Lett.*, vol. 27, no. 17, pp. 1841–1844, Sep. 1, 2015.

[11] M. Chen, J. He, J. Tang, X. Wu, and L. Chen, "Real-time 10.4-Gb/s single-band optical 256/64/16QAM receiver for OFDM-PON," *IEEE Photon. Technol. Lett.*, vol. 26, no. 20, pp. 2012–2015, Oct. 15, 2014.

[12] L. Peng, M. Hélard, and S. Haese, "On bit-loading for discrete multi-tone transmission over short range POF systems," *J. Lightw. Technol.*, vol. 31, no. 24, pp. 4155–4165, Dec. 15, 2013.

[13] F. Li, X. Li, L. Chen, Y. Xia, C. Ge, and Y. Chen, "High-level QAM OFDM system using DML for low-cost short reach optical communications," *IEEE Photon. Technol. Lett.*, vol. 26, no. 9, pp. 941–944, May 1, 2014.

[14] W. Yan *et al.*, "100 Gb/s optical IM-DD transmission with 10G-class devices enabled by 65 GSamples/s CMOS DAC core," in *Proc. OFC/NFOEC*, 2013, Paper OM3H.

[15] H. Yang *et al.*, "47.4 Gb/s transmission over 100 m graded-index plastic optical fiber based on rate-adaptive discrete multitone modulation," *J. Lightw. Technol.*, vol. 28, no. 4, pp. 352–359, Feb. 15, 2010.

[16] J. L. Wei, D. G. Cunningham, R. V. Penty, and I. H. White, "Study of 100 gigabit Ethernet using carrierless amplitude/phase modulation and optical OFDM," *J. Lightw. Technol.*, vol. 31, no. 9, pp. 1367–1373, May 1, 2013.

[17] S. Ullah *et al.*, "Optical multi-wavelength source for single feeder fiber using suppressed carrier in high capacity LR-WDM-PON," *IEEE Access*, vol. 6, pp. 70674–70684, 2018.

[18] F. Li, X. Li, J. Yu, and L. Chen, "Optimization of training sequence for DFT-spread DMT signal in optical access network with direct detection utilizing DML," *Opt. Express*, vol. 22, no. 19, pp. 22962–22967, 2014.

[19] X. Yi and K. Qiu, "Estimation and compensation of sample frequency offset in coherent optical OFDM systems," *Opt. Express*, vol. 19, no. 14, pp. 13503–13508, 2011.

[20] S. H. Müller, R. W. Bäuml, R. F. Fischer, and J. B. Hüber, "OFDM with reduced peak-to-average power ratio by multiple signal representation," *Ann. Telecommun.*, vol. 52, nos. 1–2, pp. 58–67, 1997.

[21] L. J. Cimini and N. R. Sollenberger, "Peak-to-average power ratio reduction of an OFDM signal using partial transmit sequences," *IEEE Commun. Lett.*, vol. 4, no. 3, pp. 86–88, Mar. 2000.

[22] Y. Zhou and T. Jiang, "A novel multi-points square mapping combined with PTS to reduce PAPR of OFDM signals without side information," *IEEE Trans. Broadcast.*, vol. 55, no. 4, pp. 831–835, Dec. 2009.

[23] Y. Tang, W. Shieh, and B. S. Krongold, "DFT-spread OFDM for fiber nonlinearity mitigation," *IEEE Photon. Technol. Lett.*, vol. 22, no. 16, pp. 1250–1252, Aug. 15, 2010.

[24] W. C. Meng, B. S. Thian, and T. T. Tjhung, "Distributed DFT-spread OFDM," in *Proc. IEEE Singapore Int. Conf. Commun. Syst.*, Oct./Nov. 2006, pp. 1–5.

[25] J. Ji, G. Ren, and H. Zhang, "PAPR reduction in coded SC-FDMA systems via introducing few bit errors," *IEEE Commun. Lett.*, vol. 18, no. 7, pp. 1258–1261, Jul. 2014.
[26] K. Wu, G. Ren, and M. Yu, "PAPR reduction of SC-FDMA signals using optimized additive pre-distortion," *IEEE Commu. Lett.*, vol. 19, no. 8, pp. 1446–1449, Aug. 2015.
[27] W. Lyons, "SSB/ISB systems for long-distance radiotelegraphy," *Elect. Eng.*, vol. 79, no. 2, pp. 146–149, 1960.
[28] H.-C. Chien, Z. Jia, J. Zhang, Z. Dong, and J. Yu, "Optical independent-sideband modulation for bandwidth-economic coherent transmission," *Opt. Express*, vol. 22, no. 8, pp. 9465–9470, 2014.
[29] *100G CI-BCH-4TM eFEC Technology*. Accessed: Nov. 29, 2011. [Online]. Available: http://www.Vitesse.com

YOUXU ZENG received the B.S. degree in electronic science and technology from Huaqiao University, Xiamen, Fujian, China, in 2017, where he is currently pursuing the M.S. degree in electronics and communication engineering. His main research interest includes optical communication.

ZE DONG received the joint Ph.D. degree from the Georgia Institute of Technology, USA, and Hunan University, China, in 2011. He was a Research Fellow with the Georgia Institute of Technology, from 2011 to 2014. He is currently a Professor of electrical engineering with the Department of Electronic Science and Technology, Huaqiao University, Xiamen, China. He has published over 150 papers in prestigious journals and at conference proceedings in the field of coherent optical coherent transmission systems, passive optical networks, and broadband radio-over-fiber systems. He holds ten U.S. and five Chinese patents. He was granted the "The Top Young Talents of Fujian Province" and "Fujian Province Science Fund for Distinguished Young Scholars."

YIFAN CHEN received the B.S. degree in communication engineering from the Hunan University of Science and Technology, Xiangtan, Hunan, China, in 2015. He is currently pursuing the M.S. degree in electronics and communication engineering with Huaqiao University, Xiamen, Fujian, China. His main research interest includes fiber-optic communication.

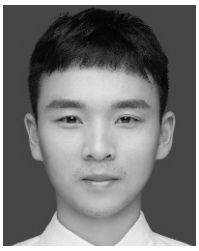

XINXING WU was born in Fujian, China, in 1993. He received the bachelor's degree from the College of Post and Telecommunication, Wuhan Institute of Technology, Wuhan, China, in 2016. He is currently pursuing the master's degree with Huaqiao University. His main research interest includes optical communication.

HAILIAN HE received the bachelor's degree in electronic information and technology from Hunan Normal University, China, in 2006, and the master's degree in circuits and systems from Hangzhou Dianzi University, China, in 2009. She is currently a Laboratory Assistant of electrical engineering with the Department of Electronic Science and Technology, Huaqiao University, Xiamen, China. Her research interest includes high-data-rate optical communication systems.

JIALIN YOU was born in Shandong, China, in 1995. He received the bachelor's degree from the College of Post and Telecommunication, Liaocheng University, Shandong, in 2017. He is currently pursuing the master's degree with Huaqiao University. His main research interest includes optical communication.

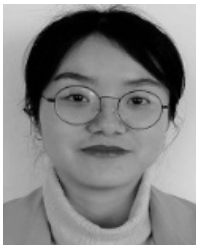

QINGHUA XIAO received the B.S. degree in optical information science and technology from the Changsha University of Science and Technology, Changsha, Hunan, in 2016. She is currently pursuing the M.S. degree in optical engineering with Huaqiao University, Xiamen, Fujian. Her research interest includes optical fiber communication systems.